

0.1 Phason elasticity and atomic dynamics of quasicrystals

F. Gähler, S. Hocker, U. Koschella, J. Roth, and H.-R. Trebin

Institut für Theoretische und Angewandte Physik,
Universität Stuttgart, D-70550 Stuttgart, Germany

0.1.1 Introduction

As the order of a quasicrystal is *quasiperiodic*, it can be described as an irrational cut through a periodic structure in a higher-dimensional space. This mathematical trick has important consequences for the low energy excitations that can occur. Translating the cut space to a different position is a symmetry operation, which changes the quasicrystal structure, but not its energy. A small breaking of this symmetry, by choosing a cut of small and slowly varying slope (with respect to the ideal orientation) therefore leads to low-energy Goldstone modes, called phasons. In many respects, phasons are analogous to phonons, which are small and slowly varying distortions of a structure in physical space. The distortions related to phasons rest in the complementary, internal space needed for the embedding of the quasicrystal in the higher-dimensional crystal.

In much the same way as there is an elastic energy for phonon type distortions of a solid, there is an effective elasticity theory for the phason degrees of freedom, which moreover is coupled to the phonon elasticity. A non-zero phason strain, i.e., a non-zero slope of the cut space, will cost energy. At higher temperatures, however, phason excitations, which correspond to a fluctuating phason strain, will become possible. This is analogous to phonons. There is one important difference, however. Whereas phonons are usually propagating modes, phasons are believed to be diffusive.

Phason strain in a quasicrystal is connected with a rearrangement of certain local atomic configurations. In an elementary form these rearrangements are called *phason flips*. Understanding the dynamics of phason flips and other atomic rearrangements of the structure of a quasicrystal is essential for the understanding of the formation and stability of quasicrystals, and also for many of their physical properties. Perfect quasicrystals are usually obtained by high temperature annealing after solidification. During this process, many defects initially present are eliminated. It is therefore necessary that phason flips, atomic diffusion, and other dynamical processes are possible and effective at these temperatures.

Atomic diffusion and phason mobility are also important for the mobility of dislocations. Unlike in a crystal, in a quasicrystal a moving dislocation leaves a phason wall in its wake. This phason wall must be smoothed out and finally eliminated by phason flips and diffusion processes, for otherwise the material would harden very quickly. Mobile phason flips are therefore necessary for the ductility of quasicrystals observed at high temperatures.

There are several other interesting consequences of phason flips. Kalugin and Katz have suggested that phason flips provide a mechanism for atomic diffusion [1]. Even though all experimental evidence indicates that vacancy mediated diffusion is dominant in quasicrystals at high temperatures [2], a phason flip mediated diffusion mechanism cannot be ruled out at lower temperatures. Blüher et al. [3] found deviations from the Arrhenius law, indicating that another diffusion mechanism becomes more efficient there. Due to phason-phonon coupling,

it should also be possible to excite phason flips by applying a mechanical stress. It is conceivable that a periodically varying mechanical stress induces phason flips, which likely lead to internal friction. Weller and Damson [4] have measured internal friction in quasicrystals, but it remains unclear whether the underlying atomic processes are related to phason flips.

Our goal here is to study *structure changing* dynamical processes in quasicrystals by means of computer simulations. Such processes are, in particular, phason flips and other jumps of atoms. We are not concerned with the long wavelength phonon part of the dynamics, which may be obtained by dynamical matrix methods [5, 6]. Our study is divided in two main parts. A first one is concerned with elasticity theory. Assuming a given atomic interaction, the elastic constants for phonons, phasons, and the phonon-phason coupling are determined for a simple model structure. It turns out that for simple, purely attractive pair potentials the matrix of elastic constants is not positive definite, i.e., the model quasicrystal is only metastable for such interactions [7]. A closer analysis suggests, however, how the potentials have to be modified to improve the situation. With the modified potentials the matrix of elastic constants becomes positive definite, at least at constant stoichiometry [8]. Unfortunately, this does not yet imply that the quasicrystal structure is the ground state. The reason is that applying a linear phason strain is not the most general deformation one can apply to a quasicrystal. Still, by Monte-Carlo simulations we find that the ground state of the modified potentials is a supertile random tiling structure very close to the perfect quasicrystal, which is a marked improvement over the original potentials. Such an analysis is an important first step in selecting interaction potentials having a quasicrystalline ground state, with which one then can perform further simulations.

On a more fundamental level, dynamical processes can be studied atomistically, by using molecular dynamics simulations. This is done in a second part. There are several ways to extract information. In principle, one can compute the Van-Hove correlation function or its Fourier transform, the dynamical structure factor, which contains all information about the dynamics. This has been attempted in [9], but it is a formidable task to do simulations providing sufficiently good statistics. This is even so if, instead of computing the whole time-averaged Van-Hove correlation function, the computation is limited to radially averaged displacement histograms at certain time intervals [9]. Often, it is therefore more promising to measure directly the quantities one is interested in.

The search for phason flips is not easy, however. One problem is that atomic jumps and flips overlap with thermal vibrations, so that special flip detectors have to be used [10]. They monitor certain local configurations and report changes. With this method it was possible to derive jump frequencies and jump distances [10]. To a certain degree it was also possible to figure out the correlation of the jumps of nearby atoms. But a full investigation would require additional tools or the computation of the correlation functions.

Another difficulty is that realistic quasicrystal models require very sophisticated potentials for their stabilization. One way to avoid this problem is to use simplified models which are stable with simple model potentials. From such simple models one can expect only qualitatively correct results, but this is still interesting. With such simple models we have studied phason flips and atomic diffusion [11], atomic jump processes [12], and even shock waves in quasicrystals [13].

Eventually, the simulation of realistic models with realistic potentials has to be mastered, however. First attempts with such potentials for decagonal Al-Cu-Co had been made in [10],

but it turned out that they were good enough only at very low temperatures. At more elevated temperatures, the Al substructure was quickly decaying, indicating that the relative energy scales of Al and transition metals is not correct. Still, it was possible to observe the expected phason flips. In this article, we report on simulations of decagonal Al-Ni-Co with newer potentials due to Moriarty and Widom [14, 15], which turn out to be much better. With these potentials, the quasicrystal is now essentially stable up to the melting point. At higher temperatures, a large part of the aluminium atoms become very mobile, so that aluminium diffusion could directly be measured. Despite this aluminium mobility, the structure remains essentially unchanged.

All the dynamical processes discussed here (phason flips, atom jumps) are candidates for the microscopic mechanisms leading to internal friction. If mechanical stress is applied to a material, the resulting deformation need not be instantaneous, because the induced atomic rearrangements need some time to complete. In the case of a periodic external stress, with a period comparable to the relevant relaxation times, this leads to a phase shift between the applied stress and the deformation, which in turn leads to dissipation. This internal friction can be observed by mechanical spectroscopy experiments [4, 16]. Direct simulation of internal friction, i.e., inducing phason flips and atom jumps by applying periodically varying mechanical stresses, has proved to be too ambitious for the moment, but understanding the candidate microscopic processes is an important step towards this goal.

0.1.2 Phason elasticity

In this section we first review the general form of linear elasticity theory for quasicrystals, and then compute all elastic constants for a simple model quasicrystal using Lennard-Jones potentials. Since not all phason elastic constants turn out to be positive [7], the potentials are then modified in a systematic way in order to make the model stable against phason strains, at least at constant stoichiometry [8]. The ground state structures of the modified potentials are determined by Monte-Carlo simulations. They turn out to be supertile random tiling structures similar to the perfect quasicrystal.

Generalized linear elasticity theory

Elasticity theory for quasicrystals describes both phonon and phason degrees of freedom. The pure phonon part is the same as for other solids. Phonon type elastic deformations are described by the Green deformation tensor

$$\varepsilon_{ij} = \frac{1}{2} \left(\frac{\partial u_i}{\partial \xi_j} + \frac{\partial u_j}{\partial \xi_i} \right), \quad (1)$$

where u_i is the displacement of an infinitesimal piece of matter with respect to its position ξ_i in the undeformed reference configuration. The deformation tensor has been symmetrized because the elastic energy does not depend on rotations of a volume element. The elastic free energy is assumed to depend analytically on the deformation. Since the reference state is the undeformed one, the linear term in the Taylor expansion vanishes. In linear elasticity theory, terms of higher than quadratic order are neglected, so that the elastic free energy density f

reads

$$f = \frac{1}{2} C_{ijkl} \varepsilon_{ij} \varepsilon_{kl} + \mathbf{O}(\varepsilon_{ij}^3). \quad (2)$$

C_{ijkl} is the Hooke tensor, and contains up to 21 independent elastic constants in the three-dimensional case, and up to 6 for two dimensions. If symmetries are present in the system, the number of independent elastic constants is reduced. For an isotropic solid, there are two independent elastic constants for both dimensions.

Besides the phonon type displacements u_i , henceforth denoted u_i^{\parallel} , for a quasicrystal there are now also displacements u_i^{\perp} in internal space, perpendicular to the physical cut space. Whereas the u_i^{\parallel} describe normal displacements of a local environment, the u_i^{\perp} describe certain internal rearrangements of an environment. Such rearrangements are called phason flips. As the rearrangement of atoms may also change the free energy, such deformations have to be included in a generalized elasticity theory for quasicrystals. Besides the Green deformation tensor ε_{ij} , here also called phonon strain, we therefore need a new deformation tensor describing the phason strain:

$$\chi_{ij} = \frac{\partial u_i^{\perp}}{\partial \xi_j^{\parallel}}. \quad (3)$$

Notice that, unlike the phonon strain, the phason strain is not symmetric in its two indices. Since the two indices refer to directions in two different spaces (internal space and physical space, respectively), the phason strain must not be symmetrized. In the general case, the free elastic energy density of a quasicrystal is

$$f = \frac{1}{2} C_{ijkl}^{\parallel,\parallel} \varepsilon_{ij} \varepsilon_{kl} + \frac{1}{2} C_{ijkl}^{\perp,\perp} \chi_{ij} \chi_{kl} + C_{ijkl}^{\parallel,\perp} \varepsilon_{ij} \chi_{kl} + \mathbf{O}((\varepsilon_{ij}, \chi_{ij})^3), \quad (4)$$

where the generalized Hooke tensor now contains $6 + 10 + 12 = 28$ independent elastic constants for a two-dimensional quasicrystal with a two-dimensional internal space.

In the presence of a non-trivial point symmetry, the number of independent elastic constants is reduced. For a two-dimensional decagonal quasicrystal, as it is considered here, the phonon strain has two symmetry invariant modes, the one-dimensional bulk deformation $\varepsilon^{(1)}$ and the two-dimensional shear deformation $\varepsilon_i^{(6)}$. The phason strain splits into two two-dimensional invariant modes, $\chi_i^{(6)}$ and $\chi_i^{(8)}$. As a consequence, a two-dimensional decagonal quasicrystal has five generalized elastic constants, the bulk modulus $\lambda_3/2$, the shear modulus $\lambda_5/2$, two phason elastic constants λ_7 and λ_9 , and a phason-phonon coupling constant λ_6 . The elastic free energy density as a function of the invariant strain modes then reads

$$\begin{aligned} f &= f_{\text{phonon}} + f_{\text{phason}} + f_{\text{coupling}} \\ f_{\text{phonon}} &= \frac{1}{2} \lambda_3 \varepsilon^{(1)2} + \frac{1}{2} \lambda_5 \left(\varepsilon_1^{(6)2} + \varepsilon_2^{(6)2} \right) \\ f_{\text{phason}} &= \frac{1}{2} \lambda_7 \left(\chi_1^{(6)2} + \chi_2^{(6)2} \right) + \frac{1}{2} \lambda_9 \left(\chi_1^{(8)2} + \chi_2^{(8)2} \right) \\ f_{\text{coupling}} &= \lambda_6 \left(\varepsilon_1^{(6)} \chi_1^{(6)} + \varepsilon_2^{(6)} \chi_2^{(6)} \right). \end{aligned} \quad (5)$$

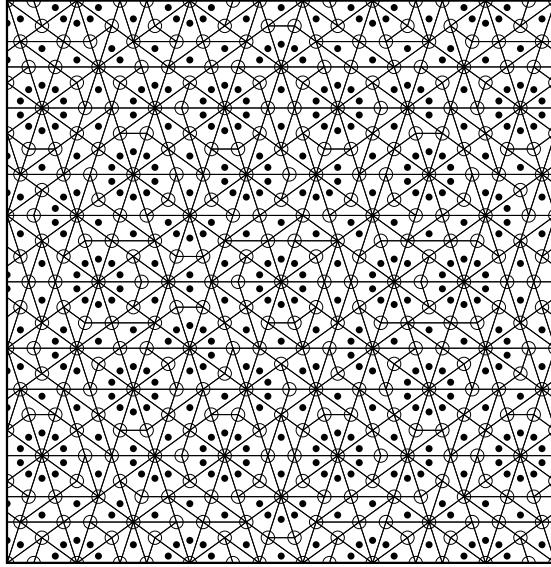


Figure 1: Mikulla-Roth binary tiling as a decoration of the Tübingen triangle tiling.

The quasicrystal model

For the atomic configuration of our two-dimensional decagonal model quasicrystal we choose the binary tiling quasicrystal of Mikulla and Roth (Fig. 1), first mentioned in [17]. Its construction based on the Tübingen triangle tiling [18] is described in [19]. This particular model has the advantage that there are unambiguous atomic configurations without defects for a wide range of phason strains, which is not the case for most other models.

For the atomic interactions we choose the Lennard-Jones potentials usually used for these binary tiling structures,

$$\phi_{ij}(r) = \epsilon_{ij} \left[\left(\frac{\sigma_{ij}}{r} \right)^{12} - 2 \left(\frac{\sigma_{ij}}{r} \right)^6 \right], \quad (6)$$

where r is the distance of the two atoms and i, j are the atom types. The parameters ϵ_{ij} and σ_{ij} are chosen such that the potential minima are at ideal nearest neighbor distances, and the minimum of the potential for different atom types is twice as deep as the other ones:

$$\epsilon_{AA} = \epsilon_{BB} = 1, \quad \epsilon_{AB} = 2, \quad \sigma_{AA} = 1.176, \quad \sigma_{AB} = 1, \quad \sigma_{BB} = 0.6180. \quad (7)$$

The purpose of the deeper minimum for different atom types is to avoid phase separation. For the simulations as well as for the analytical calculations we need to cut off the potential at some finite radius R . Furthermore, the potentials are shifted, so that they vanish at the cutoff radius R :

$$\tilde{\phi}_{ij}(r) = \phi_{ij}(r) - \phi_{ij}(R) \quad (r < R). \quad (8)$$

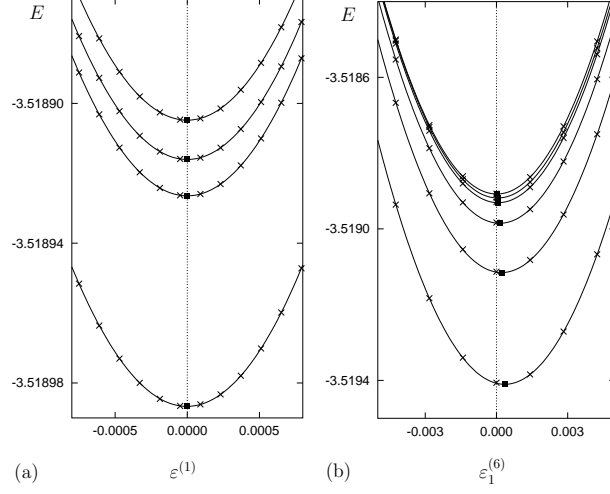


Figure 2: Elastic energy density against bulk and shear deformation for different phason strains $\chi_1^{(6)}$.

Elastic constants by molecular dynamics simulations

Our first goal is to determine the five generalized elastic constants at temperature zero for our model quasicrystal. In molecular dynamics relaxation simulations [7], we measure the minimum of the potential energy as a function of phonon and phason strain, using our molecular dynamics program IMD [20]. Up to a constant, this corresponds to the zero temperature elastic free energy. In order to avoid surface effects, we have to apply periodic boundary conditions in our simulations. We therefore need periodic structures and have to replace the quasicrystal by periodic approximants. For an approximant, on the other hand, the average phason strain has a fixed value, which is given by the geometry of the unit cell. We can thus vary the phason strain only by using different approximants, whereas the phonon strain can be varied by applying a linear transformation to the atom coordinates. For each approximant, the phonon strain with minimal energy is determined first. In a second step, the phonon strain is then varied around this value. While varying the phonon strain, the structure is permanently kept in its potential minimum.

In order to facilitate the interpretation of the simulation results, we have used approximants which have nearly pure mode phason strains, transforming either by the representations $\Gamma^{(6)}$ or $\Gamma^{(8)}$ of the decagonal point group. The bulk and shear moduli, $\lambda_3/2$ and $\lambda_5/2$, are easy to determine by applying the corresponding phonon strains to the different approximants (see Fig. 2). The phonon elastic constants correspond to the curvature of the parabolas at their minimum. They do not depend on the choice of the approximant. We also see that the minimum of the potential energy is realized for a non-zero shear deformation (see Fig. 2b), which is due to phason-phonon coupling. The position of the minimum depends only on the phason strain $\chi_1^{(6)}$, and not on $\chi_1^{(8)}$, which is in agreement with the symmetry analysis in Eq. 5. This can be seen also in Fig. 3, where the elastic energy is plotted against the two types of

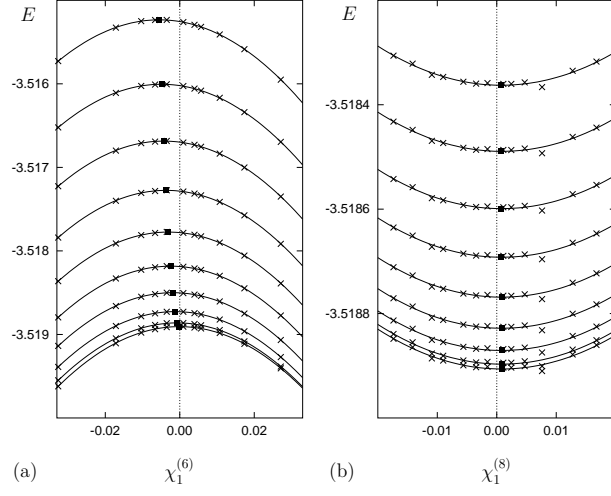


Figure 3: Elastic energy density as a function of the phason strains $\chi_1^{(6)}$ and $\chi_1^{(8)}$, for several different shear deformations $\varepsilon_1^{(6)}$.

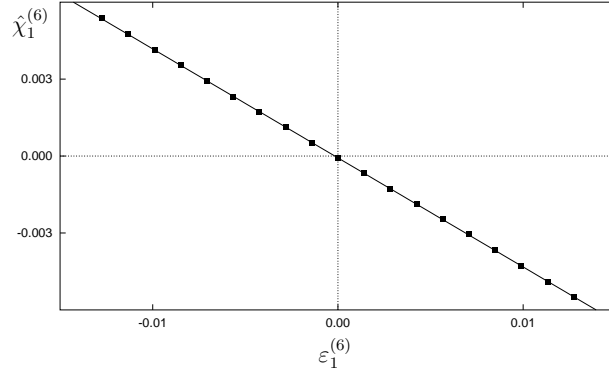


Figure 4: Extremum positions $\hat{\chi}_1^{(6)}$ from Fig. 3a as a function of the shear deformation $\varepsilon_1^{(6)}$, showing the linear behaviour of the phason-phonon coupling.

phason strain. The different curves correspond to different shear deformations. We see again, that the optimal $\chi_1^{(6)}$ phason strain depends on the given shear deformation, but not on the optimal $\chi_1^{(8)}$ phason strain. The curvatures at the extrema of the parabolas in Fig. 3 correspond to the two phason elastic constants λ_7 and λ_9 . We note that λ_7 is negative, which means that the quasicrystal is only locally stable (metastable). The phason-phonon coupling is best evaluated by plotting the extremum positions of Fig. 3a against the shear deformation (Fig. 4). This reveals a linear relationship, whose proportionality constant is $-\lambda_6/\lambda_7$, from which the phason-phonon coupling constant λ_6 can be derived.

In summary, the following values for the elastic constants are obtained for our model

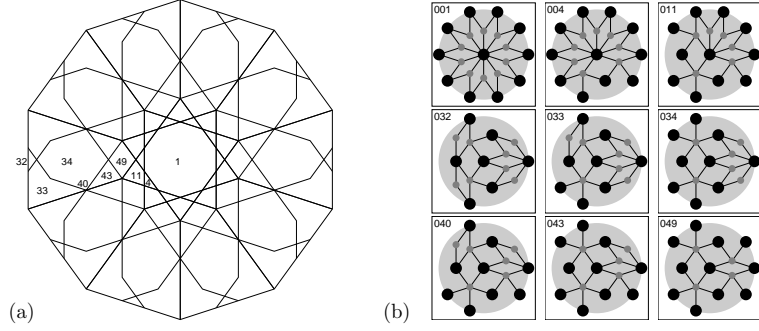


Figure 5: (a) Acceptance domains for the environments of a big atom ($R = 1.92$). An analogous subdivision exists for the acceptance domains of the small atoms. (b) Local environments of big atoms appearing in the Mikulla-Roth binary tiling quasicrystal ($R = 1.92$). No. 40 does not exist in the perfect quasicrystal, but appears already at infinitesimal phason strain.

system:

$$\begin{aligned}
 \text{phonon:} & \quad \lambda_3 = 250, & \lambda_5 = 90.2, \\
 \text{phason:} & \quad \lambda_7 = -2.70, & \lambda_9 = 0.8, \\
 \text{coupling:} & \quad \lambda_6 = -1.14. &
 \end{aligned} \tag{9}$$

Analytic computation of the phason elastic energy

In the last paragraph we have seen that the phason elastic constant λ_7 is negative, which violates the stabilization criteria and implies that the quasicrystal is metastable at temperature zero. We therefore want to analyse how the phason elastic energy depends on the potentials, in order to learn how to modify them so that they can stabilize our model quasicrystal.

For this purpose, we consider a quasicrystal with an arbitrary phason strain, but without phonon strain or local relaxation of atom positions. If we consider a cutoff radius R for the atomic interactions, the potential energy E_i of a single atom depends only on the potentials ϕ and the atomic configuration inside the ball B_{R,x_i} with radius R around the position x_i of the atom. Therefore, we can calculate the zero temperature elastic free energy by adding the potential energies of the central atoms of each local environment, multiplied by the number of occurrences N_i of the environment. In the same manner we can express the total volume by the Voronoi volumes of the central atoms of the occurring environments. We can easily rewrite this in terms of the frequencies n_i of the environments. These, on the other hand, are proportional to the areas of the acceptance domains A_i of the environments, shown in Fig. 5:

$$f = \frac{E_{\text{pot}}}{V} = \frac{\sum_i N_i E_i}{\sum_i N_i V_i} = \frac{\sum_i n_i E_i}{\sum_i n_i V_i} = \frac{\sum_i A_i E_i}{\sum_i A_i V_i}. \tag{10}$$

The energy E_i of an atom with a given environment depends only on the potentials ϕ , the corresponding acceptance domain A_i depends on the phason strain χ , and the Voronoi volumes V_i are fixed and known, so that we have derived the zero temperature free energy density

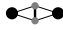

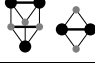



r_1	0.62	
r_2	1.00	
r_3	1.18	
r_4	1.54	
r_5	1.62	
r_6	1.90	

Table 1: Atomic distances smaller than $R = 1.92$ occurring in binary tiling quasicrystals.

$f(\chi; \phi)$ as a function of phason strain, parameterized by the values of the potentials at the occurring distances.

From now on we choose the interaction cutoff radius as $R = 1.92$. This is rather small, but includes all bonds of the characteristic tenfold cluster (Fig. 5b). For this cutoff radius there are 299 inequivalent (up to symmetry operations) local environments in a totally randomized binary tiling. 19 of them exist in the perfect quasicrystal, and another 4 occur already at infinitesimal phason strain. The remaining 276 only show up at phason strains with absolute values greater than 0.1. As we are only interested in small phason strains, and are working with linear phason elasticity theory, these latter environments are neglected.

Calculating the acceptance domains of the 23 environments of interest, and the Voronoi volumes and potential energies of the central atoms, Eq. 10 leads to

$$\begin{aligned}
 f &= f_0 + \frac{1}{2}\lambda_7\chi_6^2 + \frac{1}{2}\lambda_9\chi_8^2 + O(\chi^3) & (11) \\
 \lambda_7 &= -0.47\phi_{AA}(r_3) - 2.38\phi_{AA}(r_6) \\
 &\quad + 0.76\phi_{BB}(r_1) - 0.68\phi_{BB}(r_3) - 3.47\phi_{BB}(r_5) - 0.91\phi_{BB}(r_6) \\
 &\quad + 0.58\phi_{AB}(r_2) + 4.40\phi_{AB}(r_4) \\
 \lambda_9 &= 0.47\phi_{AA}(r_3) - 1.02\phi_{AA}(r_6) \\
 &\quad - 0.76\phi_{BB}(r_1) - 2.72\phi_{BB}(r_3) - 4.22\phi_{BB}(r_5) - 4.27\phi_{BB}(r_6) \\
 &\quad - 0.58\phi_{AB}(r_2) + 2.40\phi_{AB}(r_4).
 \end{aligned}$$

The free energy density is indeed a quadratic form in the phason strain modes, and the two phason elastic constants are now expressed as a function of the potential values at the six occurring distances shown in Table 1.

If we evaluate the phason elastic constants Eq. 11 with the Lennard-Jones potentials used for the molecular dynamics simulations, we get

$$\lambda_7 = -2.40, \quad \lambda_9 = 1.03, \quad (12)$$

while the molecular dynamics relaxation simulations resulted in

$$\lambda_7 = -2.70, \quad \lambda_9 = 0.8. \quad (13)$$

These results agree only qualitatively. One source of discrepancy is that the cutoff radius used for the simulations ($R = 7$) was bigger than the one used for the analytic expression. However, molecular dynamics simulations with the short range potential show that the difference between the two results is mainly due to atomic relaxations, which are neglected in the analytic calculations.

Modification of the potentials

Let us now have a closer look at the analytic expressions Eq. 11. The nearest neighbor interaction terms for the two phason elastic constants λ_7 and λ_9 have the same weights, but opposite sign (first column in Eq. 11). This is due to the fact, that all binary tilings with the same stoichiometry have the same potential energy, if only nearest neighbor interactions are assumed. For all plausible potentials the nearest neighbor part of λ_7 is negative, while the one of λ_9 is positive. Since the phason strain mode χ_6 increases the relative number of small atoms while χ_8 decreases it, this describes the dependence of the potential energy density on bond density.

Stoichiometry preserving phason strains satisfy $\chi_6^2 = \chi_8^2$, and thus have the phason elastic constant

$$\begin{aligned} \frac{1}{2}(\lambda_7 + \lambda_9) = & -1.70\phi_{AA}(r_6) \\ & -1.70\phi_{BB}(r_3) - 3.85\phi_{BB}(r_5) - 2.59\phi_{BB}(r_6) \\ & + 3.40\phi_{AB}(r_4). \end{aligned} \quad (14)$$

The Lennard-Jones potentials are attractive at all distances r_1 to r_6 . Thus all terms in Eq. 14 are positive, except for the last one. This term renders the system with the Lennard-Jones potentials unstable. A repulsive component in the potential between different atoms at distance r_4 makes the last term of Eq. 14 positive and leads to stabilization. As a modified potential we have chosen a mixed Lennard-Jones and Dzugutov [21, 22] potential for AB bonds, which has a minimum of -2 at distance r_2 and a maximum of $+0.25$ at approximately r_4 (Fig. 6).

The new potentials result in the following phason elastic constants:

$$\lambda_7 = -0.31, \quad \lambda_9 = 2.17, \quad (\lambda_7 + \lambda_9) / 2 = 0.93. \quad (15)$$

On the other hand, from molecular dynamics relaxation simulations with the modified potentials we obtain

$$\lambda_7 = -0.88, \quad \lambda_9 = 1.34, \quad (\lambda_7 + \lambda_9) / 2 = 0.23. \quad (16)$$

Both results indicate that with the modified potentials the quasicrystal is now stable at constant stoichiometry, but the phason elastic constant λ_7 remains negative. The calculated and simulated values of the phason elastic constants still agree only qualitatively, but have at least the same sign. In fact, the difference is now bigger than for the Lennard-Jones potentials. If we enlarge the repulsive part of ϕ_{AB} further, for example to 0.5 , we obtain from the analytic

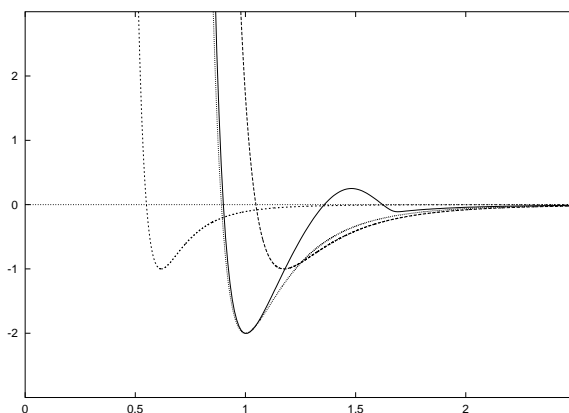


Figure 6: Original Lennard-Jones potentials and modified potential ϕ_{AB} , a mixed Lennard-Jones and Dzugutov potential.

expressions phason elastic constants which are all positive, but the simulations lead to completely different results. So, if the repulsive part is too strong, atomic relaxations overshadow completely the effect of the energy dependence on the frequencies of local environments, and the analytic calculation is no longer realistic.

Ground states by Monte-Carlo simulations

A negative phason elastic constant at temperature zero means that there exist configurations with lower potential energy, and thus the quasicrystal is not the ground state. For binary tiling quasicrystals with Lennard-Jones potentials a crystalline ground state was detected already by Lee et al. [23]. With Monte-Carlo simulations we could essentially reproduce their results. The ground state consists of an assembly of periodic nanocrystallites. We also performed Monte-Carlo simulations with the modified potentials. Here, the ground state is a supertile random tiling, with supertiles that are legal local environments from the perfect quasicrystal. However, a long range quasicrystalline order is not present, and the fat rhomb supertile seems clearly favoured (see Fig. 7). Since a tiling of only fat rhomb supertiles would lead to a different stoichiometry, some supertile defects occur to adjust the ratio of the atom types. In contrast to the simulations with Lennard-Jones potentials, the perfect quasicrystal now is a low energy configuration, even though the potential energy of the ground state as found by the Monte-Carlo simulations is clearly lower than that of the quasicrystal and its approximants.

Discussion

Our results show that with the original Lennard-Jones potentials the binary tiling quasicrystal is not stable, only metastable. For molecular dynamics simulations, this is not really a problem. Since the structure is close-packed, there are enormous energy barriers between the quasicrystal and other competing structures, which have only slightly lower energy. With

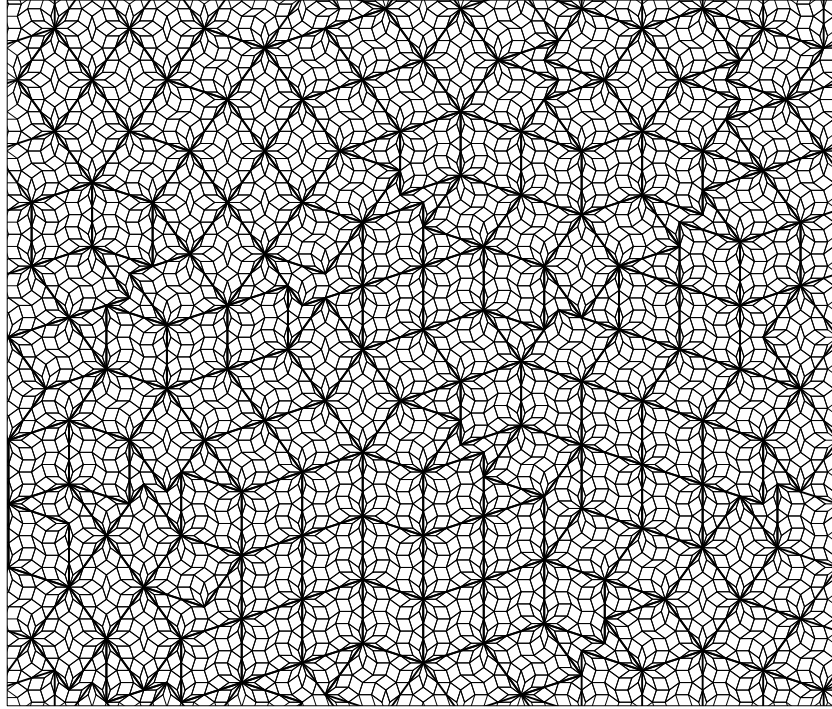


Figure 7: Ground state of the model quasicrystal with the modified potentials.

modified potentials it is possible to obtain a positive phason elastic constant for stoichiometry preserving phason strains, whereas other phason strains can still have a negative elastic constant. In fact, thermodynamic stability does not require that stoichiometry non-preserving phason strains have positive elastic constants. Rather, for stability it is required that in an energy-composition diagram the quasicrystal is an extremal state, i.e., it is on the boundary of the convex hull of the data points of all existing states (see [23]). An extremal state cannot decompose into two or more phases of lower energy, but the same average composition. So far, such an analysis has not been performed for the modified potentials.

The Monte-Carlo simulations suggest that the quasicrystal is still not the ground state, but the lowest energy states are much closer to the quasicrystal than for the Lennard-Jones potentials. The situation can certainly be improved by including interactions of longer range, but the effort for the analytical computations soon becomes overwhelming, because the number of different local environments grows rapidly with their size. We also note that the frequencies of all local environments considered vary quadratically with the phason strain, which implies that the elastic energy has also a quadratic form. A non-analytic elastic energy, as it is assumed to be necessary for an energetically stabilized quasicrystal [24], can only be obtained if the cutoff radius is larger than the matching rule radius of the tiling, which is rather big in this case [19].

The molecular dynamics simulations show that local relaxation effects are very important.

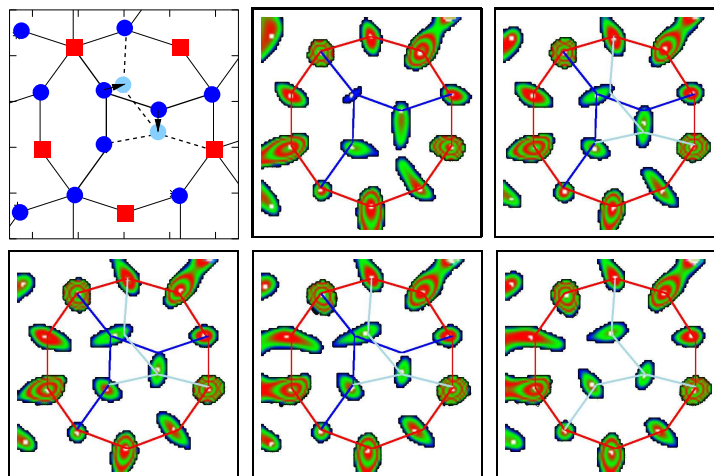


Figure 8: Top left: Drawing of phason flip in decagonal Al-Cu-Co; circles are Al, squares Cu/Co. The remaining pictures show the potential landscapes of different stages of such a flip as observed in a molecular dynamics simulation (from left to right, top to bottom). Cu/Co have deep potential minima, the flipping Al atoms only shallow, elongated ones.

They can completely overshadow the contributions from the frequencies of the (perfect) local environments. This makes an extension of the analytical computations to much larger radii doubtful. Relaxation effects also strongly modify the results from continuum elasticity theory. Atomistic considerations are therefore essential to understand the stability of quasicrystals. It is not enough to know the continuum phason elasticity.

0.1.3 Atomistic simulations

Molecular dynamics (MD) is an excellent tool for the study of dynamical processes at an atomistic level. In a MD simulation, the equations of motion of the particles in the system are integrated numerically over a sufficiently long time interval. An accurate representation of the interactions between the atoms is therefore needed. Due to the aperiodic nature of quasicrystals, any reasonable model structure requires so many atoms, that a quantum mechanical treatment of these interactions is not feasible. For this reason, classical, effective potentials have to be used. The quality of the results of MD simulations crucially depends on the quality of these potentials, and the construction of reliable potentials is a very difficult task.

MD simulations of decagonal Al-Cu-Co quasicrystals using realistic pair potentials have already been presented in [10], but the potentials were able to stabilize the model structures investigated only at very low temperatures. At higher temperatures, the Al subsystem quickly melted away, while the transition metal matrix remained stable. Hence the relative energy scales of these two subsystems were probably not correct. Still, a number of interesting results could be obtained in these simulations, among them the direct observation of a phason flip. In Fig. 8, different stages of this flip are shown, each with the potential landscape seen by the atoms involved. Cu and Co atoms are located in deep and sharp potential minima, whereas

the potential minima of the Al atoms are much shallower. Moreover, the minima of the flipping Al atoms are elongated in the direction into which the flip takes place.

In the present article, we shall concentrate on simulations carried out with new potentials derived in the framework of Moriarty's generalized pseudopotential theory (GPT) [14, 15]. These GPT potentials consist of a systematic expansion of the total energy into n -body terms, which is derived from first principles. For computational efficiency it is desirable to truncate the series as early as possible. Unfortunately, if transition metals (TM) are involved it is not always possible to terminate already after the two-body term, but Al-Lehyani et al. [25] have found that it can be done if a correction term is added to the TM-TM interactions. The correction term is fitted empirically to an ab-initio calculation of a simple quasicrystal approximant [25]. For computational efficiency, we have cut off the corrected pair potentials shortly after the third minimum, guiding the potential functions smoothly to zero. All MD simulations were carried out with the code IMD [20] developed at our institute.

Using the same corrected pair potentials, Mihalkovič et al. [26] have developed an optimized structure model of decagonal Al-Ni-Co. In Monte Carlo simulations the model was varied until a structure of minimal energy was reached. We use this model structure (with slight variations) also for our simulations. Since the model was optimized with respect to the potentials, it can be expected that they fit well together, which is important for our simulations.

Stability of the model structure

The structure model of Mihalkovič et al. [26] essentially consists of an alternating stacking of two different layers, which are decorations of the same hexagon-boat-star (HBS) tiling. The resulting periodicity is about 4 Å. Like in [26], we have worked with two different decorations which differ in stoichiometry. The simpler Ni rich decoration, shown in Fig. 9, has a composition of $\text{Al}_{70}\text{Ni}_{21}\text{Co}_9$, belonging to the "basic Ni rich" phase [27]. In the other decoration, of composition $\text{Al}_{72}\text{Ni}_{17}\text{Co}_{11}$, some of the Ni atoms are replaced by Co (see [26]). This decoration will be termed the Co rich decoration, even though it also belongs to the Ni rich corner of the existence domain of decagonal Al-Ni-Co [27]. In the following, we shall mainly concentrate on the Ni-rich decoration.

In order to check the correctness of the energy scale, we first determined the melting temperature T_m , by slowly heating the sample at constant pressure. The Ni rich sample melted at about 1250 K, whereas the Co rich sample melted at 1170 K. This is surprisingly close to the experimental melting temperature of the basic Ni rich phase of about 1200 K [27], given that the potentials were originally derived for zero temperature.

Next, to check the stability of the model structures we performed simulations at constant energy, at about $T = 0.5 T_m$. While both structures are essentially stable, there are a few Al atoms which change their positions during the first steps of the simulation. The relaxation occurs primarily inside the stars tiles: the Al atoms there move to different positions in the quasiperiodic plane, and they moreover seek alternating positions from layer to layer, breaking the 4 Å periodicity. The relaxed equilibrium positions are shown in Fig. 9. Inside the star tile, they depend on the number of boats around the star, which in turn is determined by the type of supertile in which the star is located (Fig. 9). Stars with one or three adjacent boats show an exact 8 Å periodicity in equilibrium, whereas stars with five adjacent boats show an 8 Å periodicity only up to about $0.5 T_m$. At higher temperatures all of the five equivalent positions

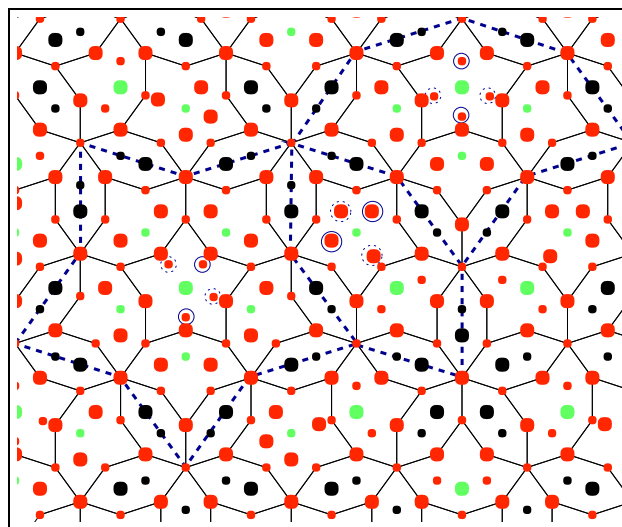


Figure 9: Ni rich decoration after relaxation. The positions of marked atoms differ from the original decoration [26]. Small (large) dots indicate atoms in upper (lower) layer. Al: dark grey; Ni: black; Co: light grey. Dashed lines mark supertiles containing the three characteristic local neighbourhoods of the star tiles. Encircled atoms occur only in every second double layer, those with solid circles in one half of the double layers, those with dashed circles in the other half.

inside the star are occupied with equal probability, and the periodicity is completely broken locally. At very high temperatures, the decoration of the hexagon supertile is further modified and becomes completely symmetric. For the following simulations, we have directly used the modified decoration corresponding the real equilibrium structure. The same modifications to the original model of Mihalkovič et al. [26] have also been observed in [28].

Aluminium diffusion

At temperatures above $0.6 T_m$, significant Al diffusion is observed (Fig. 10). Only Al atoms neighboring Co atoms are involved in the diffusion, but these form a sizeable fraction of all Al atoms. Positions with mobile Al atoms are sufficiently close to each other that long range diffusion is possible. Other Al positions can remain very stable even at high temperature, particularly those in rings with five Al and five Ni atoms. The stability of these rings can also be seen in (time averaged) atom density maps (Fig. 11), where such Al positions are very sharp, whereas those near Co atoms are completely smeared out.

As noted earlier, at temperatures close to T_m the decoration of the supertile hexagon (a boat-star pair) becomes symmetric. In the atom density maps of these supertile hexagons, one can see smeared-out parts of the Al distribution, namely pairs of banana-shaped regions near each of the Co atoms (Fig. 11), and continuous, zig-zag shaped distributions along the z-axis (Fig. 12), arising from the central dot in the supertile hexagon. These and other smeared-out parts of the Al distribution open diffusion channels. They are sufficiently close to each other

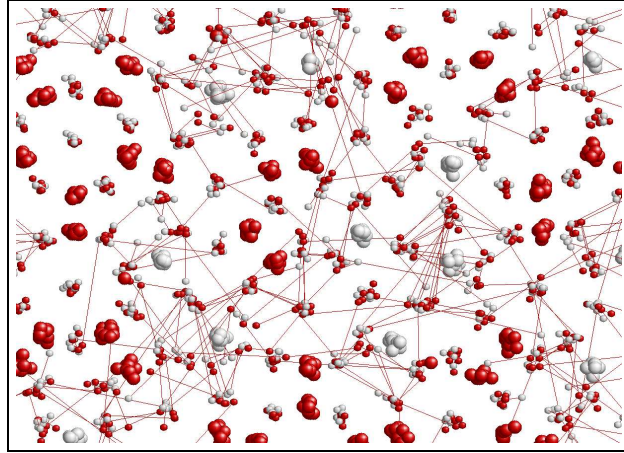


Figure 10: Al motion at $T = 0.9 T_m$. Dark grey, large: Ni; light grey, large: Co; dark grey, small: Al initial positions; light grey, small: Al positions after 1ns. Initial and final Al positions are connected.

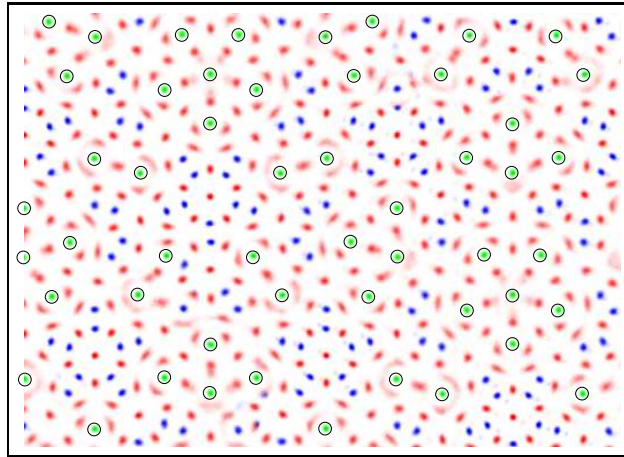


Figure 11: Atom density map, projected on xy plane. Co positions are marked with circles; Ni positions appear as sharp, almost black dots, whereas Al positions are grayish.

that long-range Al diffusion is possible. Continuous channels in the atom density maps have also been observed by Henley et al. [28]. Fig. 12 suggests that a number of aluminium atoms leave the layers, and spend considerable time between the layers. This kind of disorder could explain part of the diffuse diffraction intensity observed in x-ray scattering at high temperatures [29].

Due to the high Al diffusivities, it has been possible to measure the Al diffusion constant

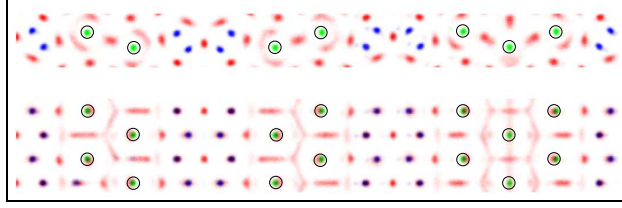


Figure 12: Atom density map similar to Fig. 11. Here, the same slab of material is shown in projections on the xy - and the xz -plane. The central dot in a supertile hexagon consists of a continuous density along a zig-zag in the z -direction, which provides a diffusion channel.

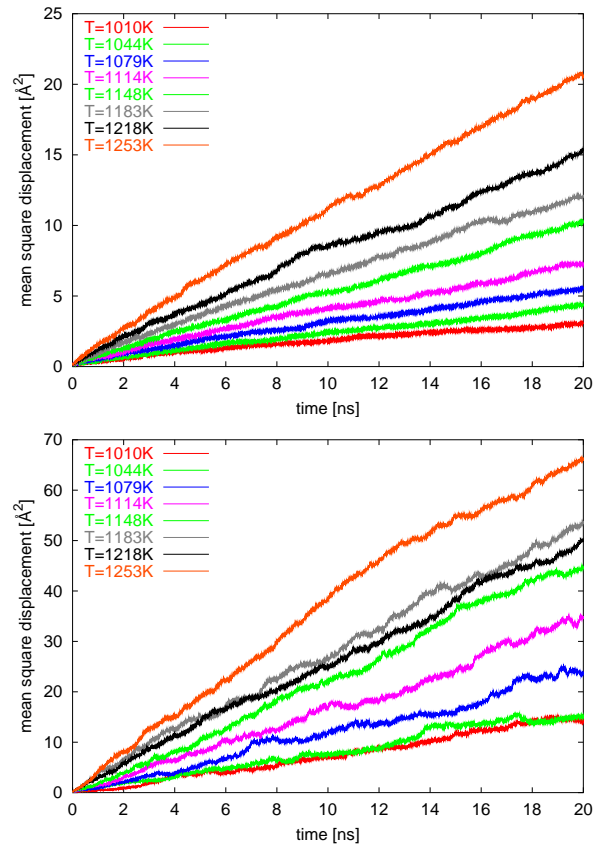


Figure 13: Mean square displacement of Al as a function of time, for different temperatures. Shown are the displacements in the x -direction (top) and the z -direction (bottom).

as a function of temperature and pressure. As expected, it follows the usual Arrhenius law:

$$D = D_0 e^{-\left(\frac{\Delta H + p\Delta V}{k_B T}\right)}. \quad (17)$$

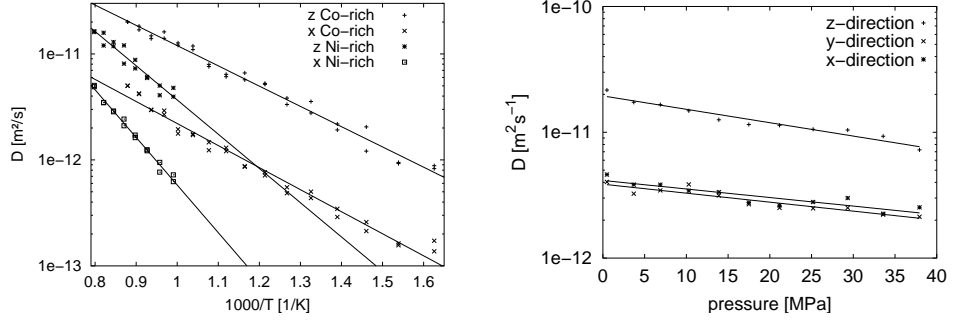


Figure 14: Left: Arrhenius plot for Al diffusion for the Ni rich and the Co rich decoration. Right: Pressure dependence of diffusion constant.

At first we chose the volume of the system corresponding to a pressure $p = 0$, and made a series of simulations with varying temperature. The resulting mean square displacements are shown in Fig. 13. From these curves (and similar ones for the Co rich decoration) the activation enthalpies H and preexponential factors D_0 could be determined, separately for the x-, the y-, and the z-direction. The resulting Arrhenius plot (Fig. 14, left) shows that the activation enthalpies are almost isotropic in the Co rich case, but somewhat anisotropic in the Ni rich case, and that both the activation enthalpies and the preexponential factors for the Ni rich composition exceed the values for the Co rich composition. Furthermore, the diffusion is isotropic in the xy-plane, as it is imposed by decagonal symmetry. The numerical values are given in Table 2.

Table 2: Activation enthalpies and pre-exponential factors for two decorations.

Decoration	Ni rich	Co rich
ΔH_{xy} [eV]	0.89	0.41
ΔH_z [eV]	0.64	0.38
D_{0xy} [m^2/s]	1.8×10^{-8}	2.6×10^{-10}
D_{0z} [m^2/s]	6.3×10^{-9}	9.8×10^{-10}

In order to determine the activation volume ΔV we performed simulations at different pressures, using the Ni rich decoration. The pressure dependence of the diffusion constants is shown in Fig. 14 (right). From the decrease of the diffusivities with increasing pressure (Eq. 17), the activation volume ΔV could be determined as 0.25Ω (quasiperiodic plane) and 0.38Ω (z-direction), where Ω is the atomic volume.

Discussion

Our results confirm that the model structure for decagonal Al-Ni-Co proposed in [26] is essentially stable up to the melting point. There are only minor modifications, in particular at

high temperatures. A sizable fraction of the Al atoms, namely those near Co atoms, become very mobile at high temperature, which leads to a high Al diffusivity, comparable to that of vacancy diffusion in fcc Al [30]. The diffusion we observe cannot be vacancy mediated, however. The activation volume we determined is too small for vacancy diffusion [31]. Moreover, there are no vacancies present in the structure, and during the short simulation time vacancies cannot form. Our results do not exclude, however, that there is also vacancy diffusion, once vacancies are present. Mehrer and Galler [31] have found that in decagonal Al-Ni-Co the diffusion of many transition metals, but also that of Zn, is predominantly vacancy mediated, as it is the case for other quasicrystals. The diffusion mechanism we observe must be due to the particular (local) structure of the quasicrystal.

Acknowledgements

We would like to thank Mike Widom and Marek Mihalkovič, who kindly provided the potentials and the initial model structures used for the atomistic simulations. This work was supported by Deutsche Forschungsgemeinschaft under Project Ro 924/4.

Bibliography

- [1] P.A. Kalugin and A. Katz, A mechanism for self-diffusion in quasi-crystals, *Europhys. Lett.* **21** (1993) 921.
- [2] H. Mehrer, R. Galler, W. Frank, R. Blüher, and A. Strom, Diffusion in quasicrystals, this volume.
- [3] R. Blüher, P. Scharwaechter, W. Frank, and H. Kronmüller, First low-temperature radiotracer studies of diffusion in icosahedral quasicrystals, *Phys. Rev. Lett.* **80** (1998) 1014.
- [4] M. Weller and B. Damson, Mechanical Spectroscopy of Quasicrystals, this volume.
- [5] M. Windisch, J. Hafner, M. Krajci, and M. Mihalkovič, Structure and lattice dynamics of rational approximants to icosahedral Al-Cu-Li, *Phys. Rev. B* **49** (1994) 8701.
- [6] M. Mihalkovič, H. Elhor, and J.-B. Suck, Atomic dynamics in Al-rich Al-Co alloys near the composition of the decagonal quasicrystal, *Phys. Rev. B* **63** (2001) 214301.
- [7] U. Koschella, F. Gähler, J. Roth, and H.-R. Trebin, Phason Elastic Constants of a Binary Quasicrystal *J. Alloys Compd.* **342** (2002) 287.
- [8] U. Koschella, F. Gähler, J. Roth, and H.-R. Trebin, Phason-elastic energy in a model quasicrystal, submitted to *J. Non-Cryst. Solids* (2002).
- [9] M. Hohl, J. Roth, and H.-R. Trebin, Correlation functions and the dynamical structure factor of quasicrystals, *Eur. Phys. J.* **B17** (2000) 595.
- [10] D. Bunz, G. Zeger, J. Roth, M. Hohl, H.-R. Trebin, Molecular Dynamic Studies of Atomic Jumps in d-AlCuCo, *Mat. Sci. Eng.* **A294-296** (2000) 675.
- [11] J. Roth and F. Gähler, Self-diffusion in dodecagonal quasicrystals, *Eur. Phys. J.* **B6** (1998) 425.
- [12] J. Roth, Jumps in Icosahedral Quasicrystals, *Eur. Phys. J.* **B15** (2000) 7.
- [13] J. Roth, Shock Waves in Quasicrystals, *Ferroelectrics* **250** (2001) 365.

- [14] J. A. Moriarty, Density-functional formulation of the generalized pseudopotential theory III. transition-metal interatomic potentials, *Phys. Rev. B*, **38** (1988) 3199.
- [15] M. Widom, I. Al-Lehyani, and J. A. Moriarty, First-principles interatomic potentials for transition-metal aluminides. III. Extension to ternary phase diagrams, *Phys. Rev. B*, **62** (2000) 3648.
- [16] H.-R. Sinning, R. Scarfone, and I.S.Golovin, Mechanical spectroscopy of hydrogen-absorbing quasicrystals, this volume.
- [17] H.-R. Trebin, R. Mikulla, J. Roth, Motion of dislocations in two-dimensional decagonal quasicrystals, *J. Non-Cryst. Solids* **153&154** (1993) 272.
- [18] M. Baake, P. Kramer, M. Schlottmann, D. Zeidler, Planar patterns with fivefold symmetry as sections of periodic structures in 4-space, *Int. J. Mod. Phys. B* **4** (1990) 2217.
- [19] F. Gähler, M. Baake, M. Schlottmann, Binary tiling quasicrystals and matching rules, *Phys. Rev. B* **50** (1994) 12458.
- [20] J. Stadler, R. Mikulla, H.-R. Trebin, IMD: A software package for molecular dynamics studies on parallel computers, *Int. J. Mod. Phys. C* **8** (1997) 1131.
See also <http://www.itap.physik.uni-stuttgart.de/~imd>
- [21] M. Dzugutov, Glass formation in a simple monatomic liquid with icosahedral inherent local order, *Phys. Rev. A* **46** (1992) R2984.
- [22] J. Roth, The fluid-solid transition of Dzugutov's potential, *Eur. Phys. J. B* **14** (2000) 449.
- [23] H. K. Lee, R. H. Swendsen, and M. Widom, Crystalline ground states of an entropically stabilized quasicrystal model, *Phys. Rev. B* **64** (2001) 224201.
- [24] H.-C. Jeong and P. J. Steinhardt, Finite-temperature elasticity phase transition in decagonal quasicrystals, *Phys. Rev. B* **48** (1993) 9394.
- [25] I. Al-Lehyani, M. Widom, Y. Wang, N. Moghadam, G. M. Stocks, and J. A. Moriarty, Transition-metal interactions in aluminum-rich intermetallics, *Phys. Rev. B*, **64** (2001) 075109.
- [26] M. Mihalkovic, I. Al-Lehyani, E. Cockayne, C. L. Henley, N. Moghadam, J. A. Moriarty, Y. Wang, and M. Widom, Total-energy-based prediction of a quasicrystal structure, *Phys. Rev. B*, **65** (2001) 104205.
- [27] S. Ritsch, C. Beeli, H.-U. Nissen, T. Gödecke, M. Scheffer, and R. Lück, The existence regions of structural modifications in decagonal Al-Co-Ni, *Phil. Mag. Lett.* **78** (1998) 67.
- [28] C. L. Henley, M. Mihalkovič, and M. Widom, Total-energy-based structure prediction for d(AlNiCo), *J. Alloys Compd.* **342** (2002) 221.
- [29] F. Frey, W. Weidner, and K. Hradil, Structural order of decagonal phases at temperatures up to 1000°, this volume.
- [30] A. Seeger, in M. T. Robinson and F. W. Young, editors, *Fundamental aspects of radiation damage in metals*, U.S. ERDA, Oak Ridge, TN (1976) 493.
- [31] H. Mehrer and R. Galler, Vacancy-mediated diffusion in quasicrystalline alloys, *J. Alloys Compd.* **342** (2002) 296.